

1.5 μm lasers with sub 10 mHz linewidth

D.G. Matei,^{1,*} T. Legero,¹ S. Häfner,¹ C. Grebing,^{1,†} R. Weyrich,¹ W. Zhang,² L. Sonderhouse,² J.M. Robinson,² J. Ye,² F. Riehle,¹ and U. Sterr¹

¹*Physikalisch-Technische Bundesanstalt, Bundesallee 100, 38116 Braunschweig, Germany*

²*JILA, National Institute of Standards and Technology and University of Colorado, Department of Physics, 440 UCB, Boulder, Colorado 80309, USA*

We report on two ultrastable lasers each stabilized to independent silicon Fabry-Pérot cavities operated at 124 K. The fractional frequency instability of each laser is completely determined by the fundamental thermal Brownian noise of the mirror coatings with a flicker noise floor of 4×10^{-17} for integration times between 0.8 s and a few tens of seconds. We rigorously treat the notorious divergencies encountered with the associated flicker frequency noise and derive methods to relate this noise to observable and practically relevant linewidths and coherence times. The individual laser linewidth obtained from the phase noise spectrum or the direct beat note between the two lasers can be as small as 5 mHz at 194 THz. From the measured phase evolution between the two laser fields we derive usable phase coherence times for different applications of 11 s and 60 s.

It is well known that frequency is the physical quantity that can be measured with by far the greatest accuracy. “Never measure anything but frequency!” was the advice of Arthur Schawlow [1]. The high accuracy results from the fact that the phase of a purely periodic signal can be measured in the simplest case by counting the zero crossings of the signal itself or with even increased accuracy by a phase measurement that interpolates the signal between the zero crossings. Hence, the generation of truly phase coherent signals over long times is the key to precision measurements and enabling technologies. In the most advanced optical atomic clocks [2–5] pre-stabilized lasers serve as oscillators to interrogate ultranarrow optical transitions with linewidths of a few mHz. Oscillators with coherence times of tens to hundreds of seconds will allow for investigations of extremely small energy shifts in the clock transition, caused by sources such as interactions amongst atoms [6, 7]. Ultrastable oscillators beyond the state of the art will find useful applications in sub-mm very long baseline interferometry (VLBI) [8], atom interferometry and future atom-based gravitational wave detection [9, 10], novel radar applications [11], the search for dark matter [12], and deep space navigation [13]. Consequently, great effort has been put into developing extremely coherent sources based on highly stable optical Fabry-Pérot resonators [14–17]. Alternative schemes are currently being investigated using cavity-QED systems [16, 18] and spectral-hole burning in cryogenic crystals [19].

Here we report on the coherence properties of two cavity-stabilized laser systems operating at a wavelength of 1542 nm. Our systems are based on well-isolated single-crystal silicon Fabry-Pérot resonators, temperature stabilized at 124 K. For a system that has well de-

signed locking electronics, the fractional frequency stability of the laser is given by the fractional stability of the optical length of the cavity. Fundamentally, the cavities’ length stability is limited by statistical Brownian noise of the mirror coatings, substrates, and spacer [20]. Due to the inherently low thermal noise of silicon crystal, the cavities’ length fluctuations are dominated by the dielectric mirror coatings, despite their thickness of only a few tens of micrometers. The cryogenic cooling of the cavities further reduces the thermal noise and allows for a fractional length instability of the cavities in the mid 10^{-17} range.

Previously, with such a system (named Si1) we demonstrated a frequency instability of 1×10^{-16} [14]. We have now set up two systems (named Si2 and Si3) and have reduced all additional noise sources [21] to a level well below the thermal noise limit.

In the following we describe briefly the set-up [22] and the analysis of the frequency stability and the phase noise. We subsequently derive methods to relate the dominant flicker frequency noise to observable and practically relevant linewidths and coherence times.

Each cavity consists of a plano-concave mirror pair employing high-reflectivity $\text{Ta}_2\text{O}_5/\text{SiO}_2$ dielectric multilayers. The finesse of the TEM_{00} mode of each cavity is close to 500 000. The 212 mm long spacer and the mirror substrates are machined from single-crystal silicon [14]. The crystal orientation of the optically contacted substrates is aligned to that of the spacer. Both have the silicon $\langle 111 \rangle$ axis oriented along the cavity axis.

The cavities are aligned vertically, and are supported at three points near the midplane in order to minimize the impact of seismic and acoustic vibrations on their length stability. The anisotropic elasticity of silicon was used to minimize the vertical vibration sensitivity below $10^{-12}/(\text{m s}^{-2})$ by adjusting the azimuthal angle between the cavity and its tripod support [21].

The cavities are placed in separate vacuum systems at a residual pressure below 10^{-9} mbar. The cavity temper-

* e-mail: dan.matei@ptb.de

† currently with TRUMPF Scientific Lasers GmbH + Co. KG, Feringastr. 10a, 85774 Unterföhring, Germany

ature is stabilized to 124 K, which is a zero crossing of the coefficient of thermal expansion of silicon [14, 21]. Each system is mounted on separate optical tables, about 3 m apart. The systems have their own active vibration isolation platforms and are surrounded by individual acoustic and temperature insulation boxes. They strongly suppress individual and thus also common noise contributions to below the thermal noise level on timescales up to several minutes [21].

Commercial Er-doped distributed feedback (DFB) fiber lasers at 1542 nm are frequency stabilized to the cavities using the Pound-Drever-Hall (PDH) method [23]. Fiber-coupled acousto-optic modulators (AOM) are used for the fast servo allowing locking bandwidths of around 150 kHz. Active residual amplitude modulation (RAM) cancellation [24] is employed to keep the corresponding fractional frequency fluctuations below the thermal noise level of the system [21].

To obtain the individual frequency instabilities of the Si2 and Si3 lasers we compared them to a third ultra-stable laser based on a 48 cm long ultra low expansion glass (ULE) cavity at 698 nm [15]. The frequency gap between the 1.5 μm Si2 system and the 698 nm ULE-cavity laser was bridged using a fiber-based optical frequency comb as a transfer oscillator [25, 26]. The comb introduces negligible noise that is below the thermal noise floor of the ULE cavity. Additional noise arising from the optical fibers connecting the lasers and the frequency comb is suppressed with active noise cancellation [27].

We measured the beat frequencies ‘Si2 – Si3’ and ‘Si2 – ULE’ using synchronized counters [28]. The third beat frequency ‘Si3 – ULE’ is calculated as their difference which is justified since our beat measurement system does not introduce appreciable additional noise.

We do not expect correlations between the ULE-cavity system, the optical frequency comb and the Si-systems, since they reside in three different rooms. Thus, the three difference frequencies allowed us to derive the three individual instabilities from a simple three-cornered hat analysis [29] (Fig. 1). The relative linear frequency drift between Si2 and Si3 of about 100 $\mu\text{Hz/s}$ (comparable with the figure reported in Ref. [30]) and between Si2 and the ULE laser of 15 mHz/s is removed.

The three-cornered hat results (Fig. 1) [32] indicate that for averaging times from 0.8 s up to 10 s the instability of each Si-based laser system is at the expected thermal noise flicker floor of $\text{mod } \sigma_y = 4 \times 10^{-17}$. This corresponds to a standard Allan deviation of about 5×10^{-17} [33]. For short averaging times the increase in the instability is due to residual vibration and acoustic noise. At long averaging times we see the effect of slow temperature fluctuations affecting the cavity length and of parasitic etalons in the optical setup.

A more complete characterization of the noise processes is given by the power spectral density (PSD) of the phase fluctuations. We have determined the phase of

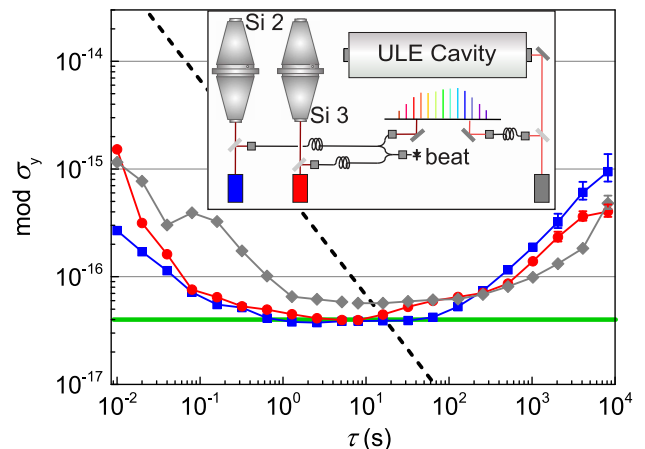


FIG. 1. (Color online) Modified Allan deviation for Si2 (squares), Si3 (circles) and ULE laser (diamonds) derived from three-cornered hat estimations. We used a 3.4 h dataset for $10 \text{ ms} \leq \tau \leq 4 \text{ s}$ and a 24.2 h dataset for $8 \text{ s} \leq \tau \leq 8192 \text{ s}$, recorded in the same day. The green line represents the expected thermal noise of the silicon cavities. For a certain evaluation model [31] the dashed line represents the instability where the rms phase fluctuations are $\sqrt{2}$ rad for a given τ . The intersections with the instability curves of the Si-lasers result in coherence times of 16 s. Linear frequency drifts in each dataset were subtracted. The inset shows a schematic of the measurement setup.

the beat signal from the measured in-phase and quadrature signal components. From more than 37 hours of phase data we determine the phase noise spectrum of a single laser down to Fourier frequencies of 0.1 mHz (Fig. 2), modeled as

$$S_{\phi}(f) = \nu_0^2 \sum_{k=-2}^0 h_k f^{k-2}. \quad (1)$$

From 1 mHz to 1 Hz the noise spectrum closely follows the thermal frequency flicker noise with $h_{-1} = 2.5 \times 10^{-33}$, in agreement with the expected thermal noise. From 1 Hz to 3 kHz the seismic and acoustic perturbations are above the thermal noise and the spectrum is approximated by white frequency noise with $h_0 = 3.6 \times 10^{-33} \text{ s}$, consistent with the increase of the instability at short averaging times (Fig. 1). Other possible sources such as photon shot-noise, RAM, laser power fluctuations are well below that level. The three broad peaks at 8 kHz, 60 kHz, and 150 kHz result from the servo loops for RAM regulation, fiber noise cancellation and PDH lock to the cavity, respectively. Below 1 mHz slow temperature fluctuations lead to a random walk frequency noise with $h_{-2} = 4 \times 10^{-36} \text{ s}^{-1}$, corresponding to the Allan deviation values above 100 s.

In the following we use this data to derive values for laser linewidth and coherence time. Usually, linewidth and coherence time are derived from the autocorrelation function of the laser field with amplitude E_0 and center

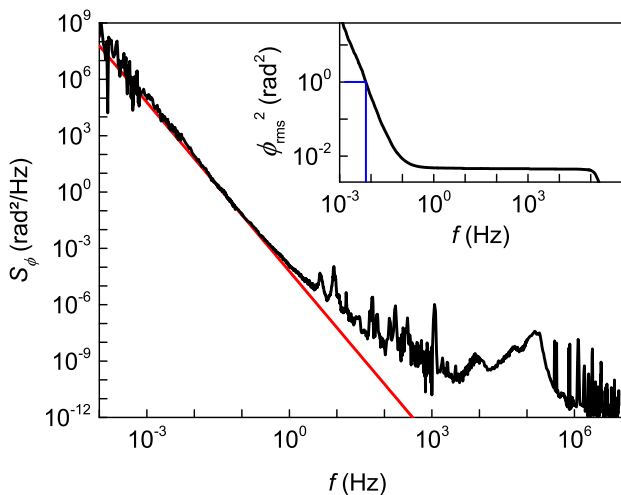


FIG. 2. (Color online) PSD of phase fluctuations of a Si stabilized laser, obtained as one half of the PSD of the Si3 – Si2 beat. The red line shows the expected flicker frequency noise corresponding to the thermal noise at $T = 124$ K. The inset shows the rms phase noise integrated down from 10 MHz. A value of 1 rad^2 is obtained after integrating down to 6.8 mHz (blue markers) leading to a FWHM linewidth of 13.6 mHz.

frequency ν_0 ,

$$R_E(\tau) = E_0^2 e^{i2\pi\nu_0\tau} e^{-1/2\langle(\phi(t+\tau)-\phi(t))^2\rangle}, \quad (2)$$

$$R_E(\tau) = E_0^2 e^{i2\pi\nu_0\tau} e^{-2\int_0^\infty S_\phi(f) \sin^2(\pi f\tau) df}. \quad (3)$$

For the flicker frequency noise and random walk frequency noise most relevant in our lasers the laser frequency $\nu(t)$ is nonstationary and $R_E(\tau)$ is divergent so that no unique coherence function can be assigned. This also leads to divergences in the general definition of the field spectrum $S_E(\delta\nu)$ as the Fourier transform of the autocorrelation function $R_E(\tau)$ (Eq. 2) and thus no uniquely defined linewidth exists. Nevertheless we can derive linewidths that are closely related to the experimental observations.

If a spectrum is recorded for a measurement of duration T_0 the linewidth is limited by the Fourier width proportional to $1/T_0$ for short measuring times whereas for longer measurement times the nonstationary frequency fluctuations broaden the line. In such a case a practical linewidth can be defined by the minimum.

To elaborate this approach Bishof *et al.* [17] make the assumption that only Fourier components of the phase noise spectrum for frequencies $f > 1/T_0$ contribute during the measurement time T_0 . From our phase noise model (Eq. 1) we obtain a minimal linewidth of $\Delta\nu_{\text{FWHM}} = 7 \text{ mHz}$ for $T_0 = 170 \text{ s}$ [34].

Experimentally we obtain linewidths from a fast Fourier transform (FFT) of the beat between the two lasers, after the beat is mixed down to a carrier frequency suitable for data acquisition. We choose 200 s measurement time to allow for sufficiently high frequency

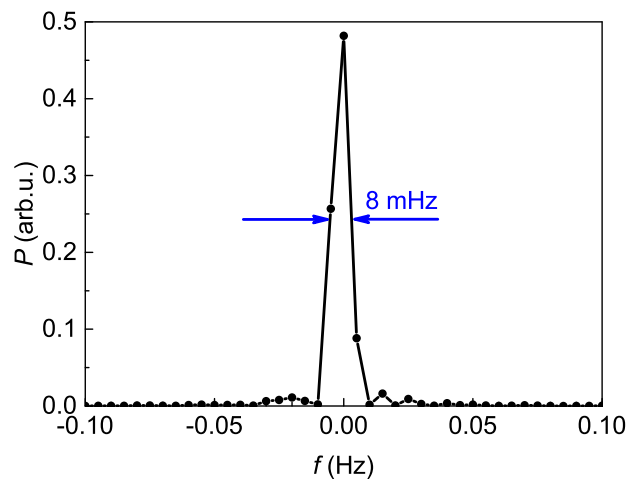


FIG. 3. (Color online) FFT spectrum of the beat note between lasers Si2 and Si3 (frequency resolution 5 mHz).

resolution while keeping the influence of slow frequency fluctuations small enough. Experimentally, in about 25% of the measurements we obtain full-width-half-maximum (FWHM) linewidths $\Delta\nu_{\text{FWHM}}$ of the beat signal between 7 mHz and 10 mHz (see Fig. 3), leading to individual linewidths as small as 5 mHz to 7 mHz, assuming that both lasers contribute equally to the linewidth. This standard approach of measuring the linewidth seems to give a reasonable agreement with the calculated minimal linewidth of 7 mHz according to [17].

To provide a linewidth estimate that includes all fluctuations of the flicker frequency noise, we averaged all FFT spectra obtained from the data set of 37 h after first aligning their centers of mass [35]. This results in an average linewidth for a single laser of about 13 mHz for a measurement time of 150 s. The difference between this longterm averaged value and the calculated minimal linewidth can be explained by the different ways the low-frequency cut-off is introduced. If a FFT spectrum analyzer is used the spectrum is centered at the average frequency during the measurement time T_0 which corresponds to a subtraction of the linear phase evolution term. Thus significant quadratic terms still contribute to the phase excursion which correspond to noise at frequencies of approximately $1/2T_0$ that is not included in the approximation of [17]. The narrower linewidths that we have observed (Fig. 3) are cases where the random quadratic term happened to be small.

Many applications are not directly sensitive to the FWHM linewidth but require sufficient spectral power in a narrow bandwidth $\Delta\nu_P$. This bandwidth can be estimated by integrating the phase noise from high-frequencies towards zero [36, 37]. The half bandwidth is obtained as the lower integration limit in

$$\int_{\Delta\nu_P/2}^{\infty} S_\phi(f) df = 1 \text{ rad}^2, \quad (4)$$

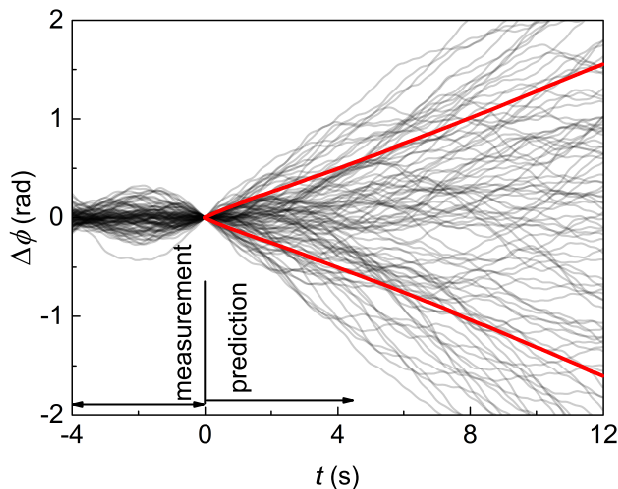


FIG. 4. (Color online) The evolution of the phase difference between the two Si lasers. The first 4 s segment is used to estimate the average frequency $\bar{\nu}$ at $t = 0$ s. For $t = 0 - 12$ s, the phase deviation from the expected $2\pi\bar{\nu}t$ is calculated. 100 consecutive curves are shown with thin gray lines. The red lines indicate the $\pm\Delta\phi_{\text{rms}}$ range, evaluated statistically from 20 750 curves.

corresponding to the case when one third of the power is contained in the bandwidth $\Delta\nu_{\text{P}}$ [37]. For this definition we find a value of $\Delta\nu_{\text{P}} = 14$ mHz (see inset of Fig. 2).

For many applications it is important to provide effective coherence times of ultrastable oscillators. For this purpose, depending on the particular application, different methods must be employed to adequately consider the nonstationary frequency. One model, widely used in VLBI [31], results in a coherence time of 16 s (Fig. 1).

As an example more adequate for optical clocks we investigate a two-pulse Ramsey interrogation of atoms. There, an average frequency and frequency drift can be estimated from past measurements and considered in the current interrogation in order to keep the phase excursions $\Delta\phi$ between the two pulses sufficiently small.

We simulate such a scenario using the phase evolution of the ‘Si2 – Si3’ beat recorded for 1 day. We cut this dataset into short samples and fit a linear phase to the first 4 s ($t = -4 \text{ s} \dots 0 \text{ s}$) to determine the average frequency $\bar{\nu}$. The phase $2\pi\bar{\nu}t$ is subtracted and the phase at $t = 0$ is set to zero to obtain the phase deviation $\Delta\phi$ for $t \geq 0$. Fig. 4 shows 100 of these samples, which indicate a time-dependent broadening. The root-mean-square deviation $\Delta\phi_{\text{rms}}(t)$ of the normally distributed phase deviation was calculated from 20 750 samples ($\pm 1\Delta\phi_{\text{rms}}$ indicated by red lines). The coherence is certainly lost when the phase has acquired an uncertainty of $\Delta\phi_{\text{rms}} \approx \pi$ (at $t \approx 30$ s) but depending on the application, more restricting definitions of the coherence time are in use. In a more conservative way we define the coherence time as a duration in which $\Delta\phi_{\text{rms}}$ has increased to 1 rad (i.e., $\sqrt{2}$ rad for the phase difference between the two indepen-

dent lasers shown in Fig. 4), leading to a coherence time of 11 s. This is equivalent to saying that after 11 s in more than 99% of all cases the actual phase excursions remain below $\pm\pi \approx 3\phi_{\text{rms}}$, which ensures unambiguous phase tracing. We find that this value of 11 s represents a broad maximum in the coherence time when the Ramsey interrogation time varies between 4 s and 20 s [38].

Besides situations where the future phase must be predicted there are many applications where the average frequency can be determined in retrospect from the measurement itself. Typical examples are spectral analysis, when the spectrum is centered, or the Rabi interrogation of atoms by single pulses, where the observed excitation provides the information of the average frequency during the measurement time. Analysis of our measured phase data shows that in this case a rms phase deviation of 1 rad occurs at measurement intervals of about 60 s, in agreement with the value estimated from the Allan deviation [38].

In conclusion, we have demonstrated the operation of two cryogenic optical silicon cavities at the thermal noise limit of $\text{mod } \sigma_y = 4 \times 10^{-17}$. The light stabilized on these cavities is highly coherent, with a coherence time of about 16 s (Fig. 1) [31]. As seen from the spectral analysis, the linewidth and implicitly the coherence time are mostly determined by the thermal noise level.

Optimizations of the current setup would hardly bring a longer coherence time since we are nearing a fundamental limit. The only way of further improving the current performance is to decrease the thermal noise even further. One approach is to decrease the temperature, thus reducing the thermal motion in the system. For an operating temperature of 4 K the expected thermal noise would be 8×10^{-18} in the modified Allan deviation. A comparable noise figure would be achieved by employing AlGaAs-based crystalline coatings, which offer a higher mechanical Q-factor and thus a lower thermal-induced noise [39, 40]. If both methods are implemented, the thermal noise would be reduced to the lower half of the 10^{-18} range, roughly an order of magnitude lower than the present level. To ensure that this improvement leads to an increased coherence time it is necessary to reduce the longterm instability for averaging times above 10 s (see intersection of dashed line with the thermal noise level in Fig. 1) while the present short-term instability seems to be sufficiently small. Our rigorous analysis of linewidth and coherence time will be tremendously important when we start using this state-of-the-art laser e.g. for investigations of classical and/or quantum correlated atoms [41]. Achieving enhanced stability from quantum correlation (such as spin squeezing) will need a local oscillator that does not introduce excessive phase noise which can easily remove the benefit of correlation [42].

This silicon cavity work is supported and developed jointly by the Centre for Quantum Engineering and

Space-Time Research (QUEST), Physikalisch-Technische Bundesanstalt (PTB), the JILA Physics Frontier Center (NSF), the National Institute of Standards and Technology (NIST). We also acknowledge support by the EU through the Horizon 2020 project Q-Sense and the European Metrology Research Programme (EMRP) under OC18. The EMRP is jointly funded by the EMRP participating countries within EURAMET and the European Union. We wish to thank E. Oelker for helpful comments about the manuscript. J. Ye thanks the Alexander von Humboldt Foundation for support. L. Sonderhouse is supported by the DoD under the NDSEG fellowship.

-
- [1] T. W. Hänsch, *Rev. Mod. Phys.* **78**, 1297 (2006).
- [2] A. D. Ludlow, M. M. Boyd, J. Ye, E. Peik, and P. O. Schmidt, *Rev. Mod. Phys.* **87**, 637 (2015).
- [3] T. L. Nicholson, S. L. Campbell, R. B. Hutson, G. E. Marti, B. J. Bloom, R. L. McNally, W. Zhang, M. D. Barrett, M. S. Safronova, G. F. Strouse, W. L. Tew, and J. Ye, *Nature Com.* **6**, 6896 (2015).
- [4] I. Ushijima, M. Takamoto, M. Das, T. Ohkubo, and H. Katori, *Nature Photonics* **9**, 185 (2015).
- [5] N. Huntemann, C. Sanner, B. Lipphardt, C. Tamm, and E. Peik, *Phys. Rev. Lett.* **116**, 063001 (2016).
- [6] A. M. Rey, A. V. Gorshkov, C. V. Kraus, M. J. Martin, M. Bishof, M. D. Swallows, X. Zhang, C. Benko, J. Ye, N. D. Lemke, and A. D. Ludlow, *Annals of Physics* **340**, 311 (2014).
- [7] M. J. Martin, M. Bishof, M. D. Swallows, X. Zhang, C. Benko, J. von Stecher, A. V. Gorshkov, A. M. Rey, and J. Ye, *Science* **341**, 632 (2013).
- [8] S. Doeleman, T. Mai, A. E. E. Rogers, J. G. Hartnett, M. E. Tobar, and N. Nand, *Publ. Astron. Soc. Pac.* **123**, 582 (2011).
- [9] J. M. Hogan and M. A. Kasevich, “Atom interferometric gravitational wave detection using heterodyne laser links,” arXiv:1501.06797v1 [physics.atom-ph] (2015).
- [10] S. Kolkowitz, I. Pikovski, N. Langellier, M. D. Lukin, R. L. Walsworth, and J. Ye, “Gravitational wave detection with optical lattice atomic clocks,” arXiv:1606.01859v2 [physics.atom-ph] (2016).
- [11] P. Ghelfi, F. Laghezza, F. Scotti, G. Serafino, A. Capria, S. Pinna, D. Onori, C. Porzi, M. Scaffardi, A. Malacarne, V. Vercesi, E. Lazzeri, F. Berizzi, and A. Bogoni, *Nature* **507**, 341 (2014).
- [12] A. Derevianko and M. Pospelov, *Nature Physics* **10**, 933 (2014).
- [13] S. Grop, P. Y. Bourgeois, N. Bazin, Y. Kersalé, E. Rubiola, C. Langham, M. Oxborrow, D. Clapton, S. Walker, J. De Vicente, and V. Giordano, *Rev. Sci. Instrum.* **81**, 025102 (2010).
- [14] T. Kessler, C. Hagemann, C. Grebing, T. Legero, U. Sterr, F. Riehle, M. J. Martin, L. Chen, and J. Ye, *Nature Photonics* **6**, 687 (2012).
- [15] S. Häfner, S. Falke, C. Grebing, S. Vogt, T. Legero, M. Merimaa, C. Lisdat, and U. Sterr, *Opt. Lett.* **40**, 2112 (2015).
- [16] M. A. Norcia and J. K. Thompson, *Phys. Rev. X* **6**, 011025 (2016).
- [17] M. Bishof, X. Zhang, M. J. Martin, and J. Ye, *Phys. Rev. Lett.* **111**, 093604 (2013).
- [18] B. T. R. Christensen, M. R. Henriksen, S. A. Schäffer, P. G. Westergaard, D. Tieri, J. Ye, M. J. Holland, J. W. Thomsen, *Phys. Rev. A* **92**, 053820 (2015).
- [19] S. Cook, T. Rosenband, and D. R. Leibbrandt, *Phys. Rev. Lett.* **114**, 253902 (2015).
- [20] K. Numata, A. Kemery, and J. Camp, *Phys. Rev. Lett.* **93**, 250602 (2004).
- [21] D. G. Matei, T. Legero, C. Grebing, S. Häfner, C. Lisdat, R. Weyrich, W. Zhang, L. Sonderhouse, J. M. Robinson, F. Riehle, J. Ye, and U. Sterr, *J. Phys.: Conf. Ser.* **723**, 012031 (2016).
- [22] See Supplemental Material, ‘Set-up: reduction of technical noise’.
- [23] R. W. P. Drever, J. L. Hall, F. V. Kowalski, J. Hough, G. M. Ford, A. J. Munley, and H. Ward, *Appl. Phys. B* **31**, 97 (1983).
- [24] W. Zhang, M. J. Martin, C. Benko, J. L. Hall, J. Ye, C. Hagemann, T. Legero, U. Sterr, F. Riehle, G. D. Cole, and M. Aspelmeyer, *Opt. Lett.* **39**, 1980 (2014).
- [25] H. R. Telle, B. Lipphardt, and J. Stenger, *Appl. Phys. B* **74**, 1 (2002).
- [26] J. Stenger, H. Schnatz, C. Tamm, and H. R. Telle, *Phys. Rev. Lett.* **88**, 073601 (2002).
- [27] L.-S. Ma, P. Jungner, J. Ye, and J. L. Hall, *Opt. Lett.* **19**, 1777 (1994).
- [28] G. Kramer and W. Klische, in *Proceedings of the 18th European Frequency and Time Forum, Guildford, UK* (IET, London, UK, 2004) pp. 595–602.
- [29] J. E. Gray and D. W. Allan, in *Proceedings of the 28th Annual Symposium on Frequency Control, 29-31 May 1974, Atlantic City, New Jersey, New Jersey* (Electronic Industries Association, 2001 Eye Street, N.W., Washington, D.C. 20006, 1974) pp. 243–246.
- [30] C. Hagemann, C. Grebing, C. Lisdat, S. Falke, T. Legero, U. Sterr, F. Riehle, M. J. Martin, and J. Ye, *Opt. Lett.* **39**, 5102 (2014).
- [31] See Supplemental Material, ‘Coherence time in radio astronomy’.
- [32] See Supplemental Material, ‘Allan deviation’.
- [33] S. T. Dawkins, J. J. McFerran, and A. N. Luiten, *IEEE Trans. Ultrason. Ferroelectr. Freq. Control* **54**, 918 (2007).
- [34] See Supplemental Material, ‘Spectral width calculations’.
- [35] See Supplemental Material, ‘FFT statistics’.
- [36] F. L. Walls and A. E. Wainwright, *IEEE Trans. Instrum. Meas.* **24**, 15 (1975).
- [37] J. L. Hall and M. Zhu, in *Laser Manipulation of Atoms and Ions*, Proceedings Internat. School of Physics “Enrico Fermi”, Vol. Course CXVIII (North Holland–Elsevier, Amsterdam, 1992) pp. 671–702.
- [38] See Supplemental Material, ‘Coherence time’.
- [39] G. D. Cole, W. Zhang, M. J. Martin, J. Ye, and M. Aspelmeyer, *Nature Photonics* **7**, 644 (2013).
- [40] G. D. Cole, W. Zhang, B. J. Bjork, D. Follman, P. Heu, C. Deutsch, L. Sonderhouse, J. Robinson, C. Franz, A. Alexandrovski, M. Notcutt, O. H. Heckl, J. Ye, and M. Aspelmeyer, *Optica* **3**, 647 (2016).
- [41] E. Paladino, Y. M. Galperin, G. Falci, and B. L. Altshuler, *Rev. Mod. Phys.* **86**, 361 (2014).
- [42] E. M. Kessler, P. Kómár, M. Bishof, L. Jiang, A. S. Sørensen, J. Ye, and M. D. Lukin, *Phys. Rev. Lett.* **112**, 190403 (2014).

Supplemental Material for 1.5 μm lasers with sub 10 mHz linewidth

SET-UP: REDUCTION OF TECHNICAL NOISE

The fractional frequency stability of the laser is directly related to the fractional stability of the optical length of the cavity. We therefore ensured that the external factors are reduced below the level given by the statistical Brownian noise. We address in the following the influence of temperature, laser power fluctuations, mechanical vibrations, and residual gas pressure fluctuations.

As temperature changes induce length fluctuations through thermal expansion, the operating point of the cryostat is chosen such that the cavity temperature precisely matches the zero-crossing point of the coefficient of thermal expansion (CTE) [S1], thus reducing the impact of temperature fluctuations. Temperature fluctuations are further reduced by enclosing the cavity in two concentric thermal shields, with the outer one being temperature-stabilized using a flow of nitrogen gas and the inner one serving as a buffer. Care has been taken also to reduce the blackbody radiation of the environment reaching the cavity, by using windows that block most of it and by limiting the solid angle through which the radiation can enter. The coefficients for the heat transfer from the room temperature environment to the inner shield and to the cavity were measured for Si3 to be $8(2) \mu\text{W}/\text{K}$ and $6(2) \mu\text{W}/\text{K}$, respectively. For the same system, the time constants for the heat flow between cavity and inner shield and inner shield and active shield are 1.3 days and 6.5 days, respectively. The temperature fluctuations of the cavity are thus reduced to below one nanokelvin for averaging times of a few seconds and affect the length stability only for times of thousands of seconds or longer [S2].

Fluctuations of the intracavity laser power lead to path length fluctuations due to heating caused by the absorbed power. We measured a value of $1.7(2) \times 10^{-15} (\mu\text{W})^{-1}$ for both cavities for the proportionality coefficient between fractional frequency and transmitted power fluctuations. The coefficient is small because the cavity is operated near the zero CTE point of the mirror substrates and due to their high thermal conductivity, and thus no active control of the intensity is needed.

Vibrations transmitted to the cavity can change its dimensions, leading to frequency instability. Thus we minimized the sensitivity to accelerations in all directions by employing a stiff holding frame. In addition, the sensitivity to vertical accelerations was experimentally minimized by changing the angle between the three point support and the crystalline axis [S2]. The acceleration sensitivities are summarized in Table I.

TABLE I. Acceleration sensitivities for the Si2 and Si3 cavities.

System	sensitivities ($10^{-12} / \text{ms}^{-2}$)		
	k_x	k_y	k_z
Si2	2.5(12)	0.7(6)	0.4(5)
Si3	8.6(7)	4.0(2)	0.8(5)

Combined with the measured seismic vibrational spectrum, this ensures that the vibration-induced frequency noise is below the thermal-noise limit for averaging times above 100 ms [S2].

Fluctuations in the residual gas pressure present in ion pumps [S3] also induce frequency instabilities by changing the refractive index of the residual gas between the mirrors and thus altering the optical length. Using ultra-high-vacuum compatible materials and keeping the ion pumps always in the low pressure range, we achieve a stable base pressure of 10^{-9} mbar. From the observed pressure fluctuations we estimate that corresponding frequency fluctuations are below 4×10^{-17} for averaging times shorter than a few thousand seconds.

ALLAN DEVIATION

The modified Allan deviation (mod ADEV) is used to characterize the frequency stability. It reduces the impact of high frequency phase noise on the stability values at longer averaging times, as our beat signals contain phase noise at high frequencies that arises from the frequency comb [S4] and from laser noise at frequencies above the bandwidth of the PDH locks. The modified Allan deviation also enables to distinguish different types of noise that are typically indistinguishable in the Allan deviation [S5, S6].

The modified Allan deviation requires frequency counters that temporally average the frequency fluctuations with a triangular weighting function (so-called Λ -counters [S7, S8]). As our counters [S9] only approximate the Λ -sensitivity from 1 ms measurements with constant weighting function (Π -counter), we additionally band-pass filter the signals with bandwidths of about 1 kHz to better approximate the correct sensitivity function.

SPECTRAL WIDTH CALCULATIONS

The Wiener-Khinchine theorem relates the field spectrum S_E to the Fourier transform of the field autocorrelation function

$$R_E(\tau) = \langle E(t+\tau)E^*(t) \rangle. \quad (\text{S1})$$

For a field $E(t) = E_0 e^{2\pi i \nu_0 t} e^{i\phi(t)}$ with average frequency ν_0 and random phase $\phi(t)$ this autocorrelation function can be expressed as

$$R_E(\tau) = E_0^2 e^{2\pi i \nu_0 \tau} \exp\left(-\frac{1}{2} \Delta\phi_{\text{rms}}^2(\tau)\right) \quad (\text{S2})$$

where we have used the root-mean-square (rms) phase increment

$$\Delta\phi_{\text{rms}}^2(\tau) = \langle (\phi(t+\tau) - \phi(t))^2 \rangle. \quad (\text{S3})$$

The phase increment can be calculated with a sensitivity function

$$h^{(\tau)}(t) = \delta(t-\tau) - \delta(t) \quad (\text{S4})$$

as

$$\phi(t+\tau) - \phi(t) = \int \phi(t+t')h(t')dt', \quad (\text{S5})$$

using the Dirac delta function $\delta(t)$. With the help of Parseval's theorem, the rms value of this convolution can be expressed through the power spectral density of phase fluctuations $S_\phi(f)$ as

$$\Delta\phi_{\text{rms}}^2(\tau) = \int_0^\infty S_\phi(f) |H(f)|^2 df \quad (\text{S6})$$

$$= 4 \int_0^\infty S_\phi(f) \sin^2(\pi f \tau) df \quad (\text{S7})$$

where the Fourier transform of the sensitivity function $h(t)$

$$H(f) = \int_0^{T_0} h(t) \exp(2\pi i f t) dt \quad (\text{S8})$$

is used.

With the power spectral density of frequency fluctuations $S_\nu(f) = f^2 S_\phi(f)$ the corresponding autocorrelation function reads

$$R_E(\tau) = E_0^2 e^{2\pi i \nu_0 \tau} \exp\left(-2 \int_0^\infty S_\nu(f) \frac{\sin^2(\pi f \tau)}{f^2} df\right). \quad (\text{S9})$$

However, for frequency noise processes $S_\nu \propto f^k$ that are diverging towards zero frequency with $k \leq -1$, this autocorrelation function is diverging. This is due to the fact that the phase difference, expressed by the average frequency $\bar{\nu}_\tau(t)$ in the interval $[t, t+\tau]$

$$\Delta\phi(t) = \phi(t+\tau) - \phi(t) \quad (\text{S10})$$

$$= 2\pi\tau\bar{\nu}_\tau(t) \quad (\text{S11})$$

is nonstationary, so the expectation values needed for the definition of the autocorrelation function R_E does not exist.

A similar problem appears when trying to use the classical frequency variance $\langle \bar{\nu}(t)^2 \rangle$ to describe the stability of oscillators in time domain [S10]. There the Allan variance σ_ν^2 is now widely used instead to describe the stability of such sources, which circumvents the divergence of the classical variance by taking the variance between successive average frequencies:

$$\sigma_\nu^2(\tau) = \frac{1}{2} \langle (\bar{\nu}_\tau(t+\tau) - \bar{\nu}_\tau(t))^2 \rangle. \quad (\text{S12})$$

Low-frequency cutoff methods

As only finite observation times T_0 are used in any real experiment, it is common to avoid the divergence by introducing low-frequency cutoffs f_{co} in Eq. (S9). In the work of Stephan *et al.* [S11] a cutoff at $f_{\text{co}} = 1/\tau$ is introduced. For pure flicker noise $S_\nu = h_{-1} f^{-1}$ this approach leads to a Gaussian line profile and an effective FWHM linewidth $\Delta\nu = 0.3537\nu_0\sqrt{h_{-1}}$ independent of observation time.

Bishop *et al.* [S12] introduce a cutoff at $f_{\text{co}} = 1/T_0$, which leads to a linewidth that depends on the observation time T_0 , and its minimum is used as the effective linewidth. To include also the Fourier width due to the limited observation time, windowing functions $w(t)$ are employed in the finite-length Fourier transform [S13], leading to a spectrum of

$$S_E(f) = \int_0^\infty W(\tau) R_E(\tau) \cos(2\pi f \tau) d\tau. \quad (\text{S13})$$

Here the weighting function for the autocorrelation function $W(\tau)$ is the convolution of the initial weighting function with itself $W(\tau) = (w * w)(\tau)$. E.g. in the case of a rectangular window function of duration T_0 it is

$$W(\tau) = (1 - |\tau|/T_0). \quad (\text{S14})$$

Practical spectral measurements

The above methods do not directly correspond to practically employed spectral measurements. One widely used method to measure an effective linewidth is the spectral analysis of the beat signal between two similar oscillators during a limited measurement duration T_0 using spectrum analyzer [S14], often based on a Fast Fourier Transform (FFT) of the signal. Here naturally only the width is recorded, while the average frequency of the beat is manually tracked to keep the signal within the observation bandwidth, which compensates for the nonstationary frequency of flicker noise. E.g. for a spectral measurement of duration T_0 , the average frequency

can be determined from the spectrum itself as the central frequency of the observed spectral feature.

Mathematically, this means that no longer the complete phase evolution $\phi(t)$ is analyzed over infinite durations. Instead the expectation value of finite duration spectra from $\phi^{(\text{cor})}(t)$ are considered, where the phase $\phi^{(\text{av})}(t)$ due to the average frequency ν^{av} is subtracted from each individual spectrum. Thus the variance of the phase increments in Eq. (S3) is not taken from the real laser phase but for the phase increments corrected by an average phase increment $2\pi\nu^{(\text{av})}(t_2 - t_1)$ during the observation time with an average frequency $\nu^{(\text{av})}$.

Steck [S15] uses a weighted averaging depending on τ and T_0 to obtain a FWHM as function of T_0 . Its minimum for flicker noise $S_\nu(f) = h_{-1}/f$ is $0.5\nu_0\sqrt{h_{-1}}$ at $T_0 = 14\nu_0/\sqrt{h_{-1}}$.

It should be noted that, due to this subtraction, the corrected phase increment in the observation interval in general is no longer invariant to time translation, but now depends on the two times: $\Delta\phi(t_1, t_2)$. The finite-length spectrum (periodogram) with window function $w(t)$ is given as absolute squared Fourier transform of the signal:

$$S_E(f) = |\mathcal{F}_E(f)|^2 \quad (\text{S15})$$

$$= \int_0^{T_0} \int_0^{T_0} w(t_1)w(t_2)e^{-\frac{1}{2}\Delta\phi^2(t_1, t_2)} \quad (\text{S16})$$

$$\cdot \cos(2\pi f(t_2 - t_1))dt_1dt_2. \quad (\text{S17})$$

In the simplest way, the average frequency can be calculated from the phase increment during the interval $[t, t + T_0]$:

$$\phi^{(\text{av})} = 2\pi\tau\bar{\nu}(t) = \phi(t + T_0) - \phi(t). \quad (\text{S18})$$

The sensitivity function that corresponds to this interpolation by the average frequency is

$$h^{(\text{int})}(t_1, t_2) = (t_2 - t_1)/T_0(\delta(t - T_0) - \delta(t)), \quad (\text{S19})$$

with the corresponding Fourier transforms

$$H^{(\tau)}(t_1, t_2, f) = e^{2\pi ift_2} - e^{2\pi ift_1}, \quad (\text{S20})$$

$$H^{(\text{int})}(t_1, t_2, f) = (t_2 - t_1)/T_0(e^{2\pi ifT_0} - 1), \quad (\text{S21})$$

$$H^{(\text{diff})}(t_1, t_2, f) = H^{(\tau)}(t_1, t_2, f) - H^{(\text{int})}(t_1, t_2, f) \quad (\text{S22})$$

The rms phase variations $\Delta\phi_{\text{rms}}(t_1, t_2)$ is thus expressed with the help of Parseval's theorem as:

$$\Delta\phi_{\text{rms}}(t_1, t_2) = \int_0^\infty S_\phi(f) \left| H^{(\text{diff})}(t_1, t_2, f) \right|^2 df, \quad (\text{S23})$$

and the field autocorrelation with a window function $w(t)$ for $\tau > 0$:

$$R_E(\tau) = E_0^2 \int_0^{T_0-\tau} w(t) w(t + \tau) e^{-\frac{1}{2}\Delta\phi_{\text{rms}}(t, t+\tau)} dt. \quad (\text{S24})$$

A better approximation to the average frequency is a least square fit to the laser phase, weighted by the window function $w(t)$ of the FFT. Without loss of generality we consider the interval $[0, T_0]$. For the fit we use a sum of orthogonal polynomials $\Pi_k(t)$ over the interval $[0, T_0]$ with weight $w(t)$. For constant weight $w = 1$ these are the shifted Legendre polynomials. Then in the least-square sense the phase is approximated by

$$\phi^{\text{fit}}(t) = \sum_{k=0}^N c_k \Pi_k(t), \quad (\text{S25})$$

with coefficients

$$c_k = \int_0^{T_0} w(t) \Pi_k(t) \phi(t) dt. \quad (\text{S26})$$

Thus these coefficients can be expressed as convolution between the phase $\phi(t)$ and a kernel $w(t)\Pi_k(t)$, thus the variance of the corrected phase can be expressed with the help of Parseval's theorem through the product of S_ϕ and the square of the absolute value of the Fourier transform $\mathcal{F}(w(t)\Pi_k(t))$.

The rectangular (constant) weighting window and the Hanning window [S13]

$$w(t) = 1 - \cos(2\pi t/T_0) \quad (\text{S27})$$

are widely used in FFT spectral analysis. For both window functions we have calculated the phase variance (Fig. S1) and the linewidth as function of the measurement interval length T_0 (Fig. S2 (closed symbols) and Fig. S3). If only the linear phase is fitted ($N = 1$), we expect to obtain the linewidth of the averaged spectra. If the fit also includes a quadratic term ($N = 2$), we expect to find the minimum observed linewidth, as during these measurements the actual frequency drift (i.e. the quadratic phase) was close to zero.

FFT statistics

For a complete characterization of the linewidth measurements with FFT we used the 37 h phase record used for calculating the phase noise spectrum. The data was broken up in adjacent equal-length segments and a FFT spectrum was obtained for each of them. The spectra were aligned on the frequency axis such that their center of mass is at 0 Hz. For a finer alignment, the resolution bandwidth of the FFT calculation was increased artificially by zero-padding the segments up to eight times their length. For each frequency the mean value from all spectra was calculated, resulting in an averaged spectrum as displayed in Fig. S4. When varying the length of the segments we obtain the data shown in Fig. S2 with open symbols. It results that the optimum interval length for obtaining a minimal linewidth lies between 120 s and 150 s.

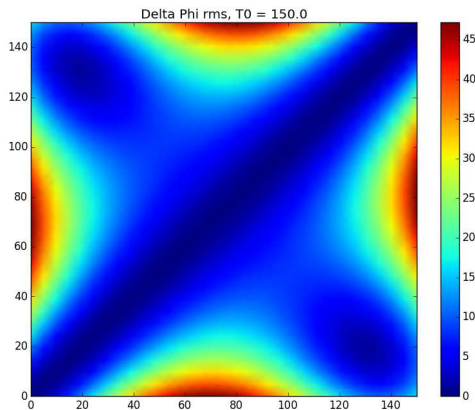


FIG. S1. Phase deviation $\Delta\phi_{\text{rms}}(t_1, t_2)$ for the experimentally observed spectrum of frequency fluctuations, a duration $T_0 = 150$ s and a fit with rectangular weighting function.

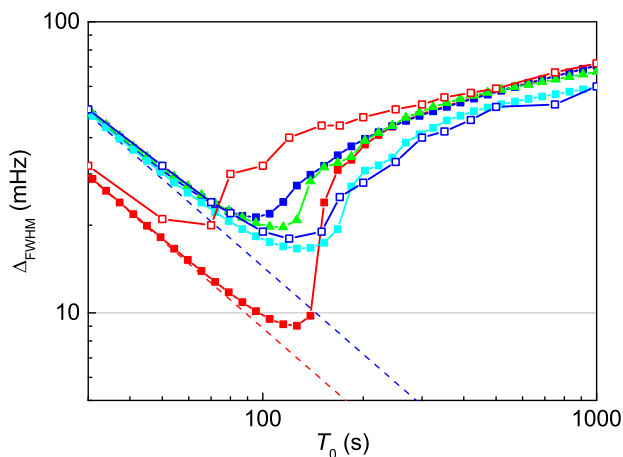


FIG. S2. FWHM beat linewidth Δ_{FWHM} as a function of observation time T_0 . Filled symbols: Calculations using the modeled phase noise spectrum and different methods to deal with the low-frequency divergence: with a cutoff at $f = 1/T_0$ [S12] and rectangular window (red squares) or Hanning window (blue squares), with subtraction of phase frequency from weighted linear fit and Hanning window (green triangles) and with weighted quadratic fit and Hanning window (cyan squares). Open symbols: Linewidths obtained by averaging FFT spectra obtained with different window functions: rectangular (red squares) and Hanning (blue squares). The dashed lines indicate the respective Fourier limits of the rectangular (red) or Hanning window (blue).

Since the individual FFT spectra usually have irregular shapes to which no analytic peak function can be assigned, we use an empirical approach in estimating their linewidths. First the maximum value was determined. Then the maximum was approached from both ends of the spectrum until the half-value was encountered. The difference between the two frequency values was then taken as the FWHM value. Using the data from Fig.

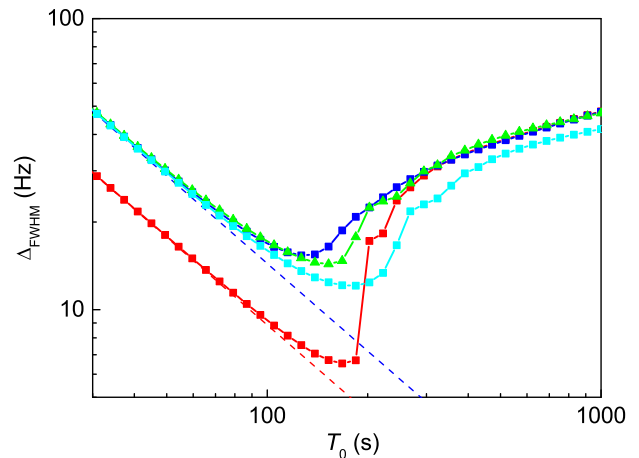


FIG. S3. Single laser FWHM linewidth Δ_{FWHM} as a function of observation time T_0 calculated from the modeled phase noise spectrum. For plot legend see caption of Fig. S2.

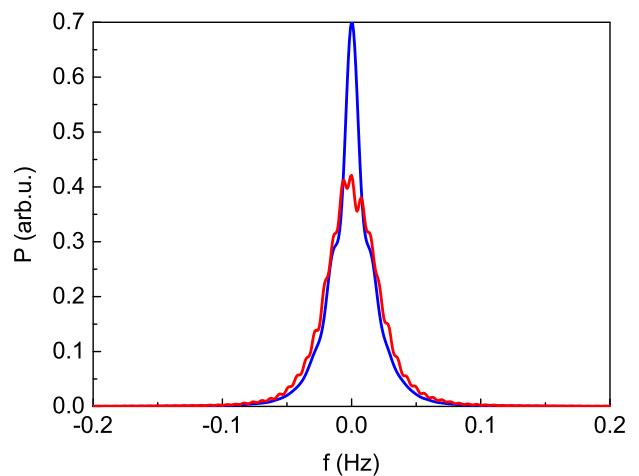


FIG. S4. Averaged FFT spectrum of the beat of the two lasers obtained from a phase measurement of 37 h by averaging all spectra obtained from 150 s intervals with a rectangular window (red line) and Hanning window (blue line). The increased frequency resolution comes from zero-padding the data before the FFT calculation.

S4 we obtain a linewidth of 19 mHz (for a Hanning window) of the beat, which results in a single-laser average linewidth of about 13 mHz.

We also calculate the distribution of linewidths over the time span of 37 h. The result is shown in the upper graph from Fig. S5 for an interval of 200 s. This corresponds to the measurement with a FFT analyzer shown in the main text. The highlighted part represents the linewidths below 10 mHz which amounts to 25% of all measurements. For comparison, the same analysis for a simulated pure flicker frequency noise is shown in the lower graph. The similarity of the two histograms confirms once again that in this time range the behavior of the lasers is essentially described by a flicker frequency

noise and that the broad distribution of linewidths is intrinsic to $1/f$ noise and not due to additional technical perturbations.

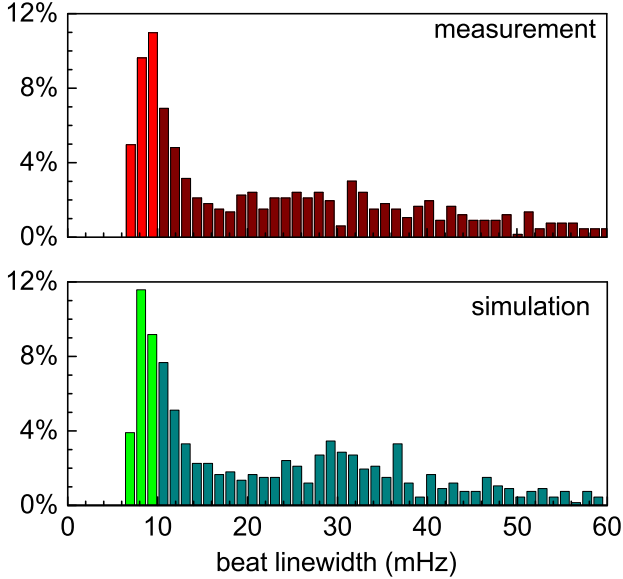


FIG. S5. Histogram of spectral linewidths for measured beat data (upper graph) and simulated flicker frequency noise (lower graph) corresponding to 200 s segments obtained from a 37 h record.

COHERENCE TIME

The coherence time T_{co} can be defined [S16] as the time where the autocorrelation function $R_E(\tau)$ has fallen to a certain fraction (e.g. $1/2$ or $1/e$) of its value at $\tau = 0$. According to Eq. (S2) the definition of coherence time T_{co} by $R_E(T_{\text{co}}) = 1/e$ corresponds to $\Delta\phi^2(T_{\text{co}}) = 2 \text{ rad}^2$.

A relation between coherence time and FWHM linewidth $\Delta\nu$ can be found in [S16] which gives $T_{\text{co}} = 1/\Delta\nu$ for rectangular, $T_{\text{co}} = 0.32/\Delta\nu$ for Lorentzian and $T_{\text{coh}} = 0.66/\Delta\nu$ for Gaussian spectra.

Coherence time for Ramsey interrogations

For Ramsey spectroscopy, the frequency of the interrogating laser needs to be measured in advance. Depending on this measurement time, the quality of the predicted phase evolution and thus the coherence times may change. Using the measured phase date, we have calculated the corresponding coherence time as a function of the preceding measurement time. As shown in Fig. S6, the coherence time is close to the maximum value of 11 s for measurement times between 4 s and 20 s.

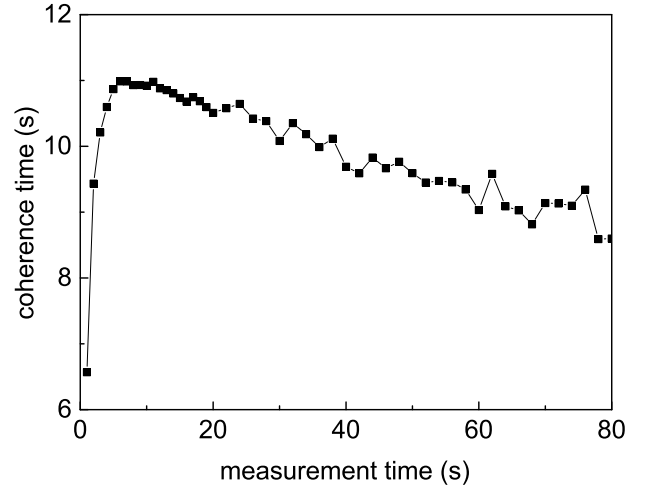


FIG. S6. Coherence time for Ramsey interrogation calculated for different lengths of the preceding measurement interval.

Coherence time for Rabi interrogations

For a Rabi interrogation the frequency of the laser does not need to be known in advance but can be determined after the measurement from the result of the measurement itself. The coherence time resulting from the phase fluctuations can be measured as indicated in Fig. S7. The same dataset as used above is divided in equal-length intervals and from each interval, the average frequency $\bar{\nu}$ is calculated and its corresponding phase evolution is subtracted from the data. The coherence time is defined as the interval length for which the remaining average phase fluctuations are less than $\sqrt{2}$ rad. From our data we find a value of 60 s.

Relation between Allan deviation and coherence time

To predict the future phase under the condition of non-stationary frequency fluctuations, as in the case of flicker and random walk frequency noise, the future frequency needs to be estimated using an average frequency from the past values. As a convenient way for extrapolation over a duration τ in an interval $[t, t + T_0]$, the average frequency from the preceding interval with the same duration $[t - T_0, t]$ can be used. The variance between successive frequencies is used in the definition of the Allan deviation

$$\sigma_y^2(\tau) = \frac{1}{\nu_0^2} \left\langle \frac{1}{2} (\bar{\nu}_{i-1} - \bar{\nu}_i)^2 \right\rangle \quad (\text{S28})$$

$$= \frac{1}{4\pi^2 T_0^2 \nu_0^2} \left\langle \frac{1}{2} (\Delta\phi_{i-1} - \Delta\phi_i)^2 \right\rangle, \quad (\text{S29})$$

where ν_0 denotes the average frequency, and $\bar{\nu}_i$ the average frequency over the interval of duration τ , $\langle \cdot \rangle$ the

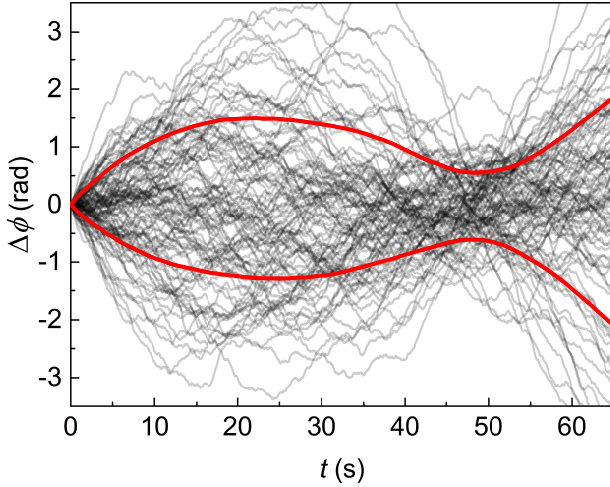


FIG. S7. The evolution of the phase difference between the two Si lasers. The measured phase of 100 consecutive curves is shown with thin gray lines. The average frequency $\bar{\nu}$ calculated for each curve is already subtracted. The remaining rms fluctuations are below $\sqrt{2}$ rad in average for intervals up to 60 s long. The red lines indicate the $\pm\Delta\phi_{\text{rms}}$ range, calculated from 1 300 curves.

expectation value. If the frequency is adjusted to the frequency of the preceding interval, this corresponds to $\Delta\phi_{i-1} = 0$, and thus

$$\Delta\phi_{\text{rms}}^2 = 8\pi^2\nu_0^2 T_0^2 \sigma_y^2(\tau) = \langle \Delta\phi_i^2 \rangle. \quad (\text{S30})$$

On the other hand, if the average frequency $\bar{\nu}$ is determined from the measurement itself using $\bar{\nu} = (\phi(t+T_0) - \phi(t))/2\pi T_0$, the maximum phase excursion is expected at the midpoint of the interval $t + T_0/2$ and its variance is given by

$$\Delta\phi_{\text{rms}}^2 = \left\langle \left(\phi(t + T_0/2) - \frac{\phi(t + T_0) - \phi(t)}{2} \right)^2 \right\rangle, \quad (\text{S31})$$

which is

$$\Delta\phi_{\text{rms}}^2 = 1/4 \cdot (2\pi T_0/2)^2 \langle (\bar{\nu}_i - \bar{\nu}_{i+1})^2 \rangle, \quad (\text{S32})$$

where $\bar{\nu}_i$ and $\bar{\nu}_{i+1}$ denote the average frequency over the intervals $[t, t + T_0/2]$ and $[t + T_0/2, t + T_0]$.

This can be expressed by the Allan deviation as:

$$\Delta\phi_{\text{rms}}^2 = \pi^2 T_0^2 \nu_0^2 \sigma_y(T_0/2)/2. \quad (\text{S33})$$

In the case of flicker noise, the corresponding coherence time T_0 is longer by a factor of $\sqrt{8}$ compared to the case where the average frequency is predicted from past values only (Eq. S30).

Coherence time in radio astronomy

In radio astronomy the coherence time τ_{co} of an oscillator with frequency ν_0 is commonly estimated from the standard Allan deviation σ_y [S17–S19]:

$$2\pi\nu_0 \tau_c \sigma_y(\tau_c) = 1. \quad (\text{S34})$$

Comparing to Eq. (S30), this approach corresponds to a definition of coherence time, where the rms phase excursion is $\sqrt{2}$ radian. It seems the difference of the phase variance by a factor of two from Eq. (S30) is due to a different, not commonly used definition of the Allan deviation without a factor of 1/2 used in [S17–S19].

From the measured flicker floor of $\text{mod } \sigma_y = 4 \times 10^{-17}$ (corresponding to standard Allan deviation $\sigma_y = 5 \times 10^{-17}$) according to this definition we find a coherence time of about 16 s for the Si-stabilized lasers.

The condition of Eq. (S34) can be illustrated in the stability diagram, shown in Fig. 1 as the intersection between the Allan deviation curve and the $1/\tau$ line corresponding to Eq. (S34). It is clear that for both lasers the coherence time is determined by the flicker floor, given by the thermal noise of the cavities.

-
- [S1] T. Middelmann, A. Walkov, G. Bartl, and R. Schödel, *Phys. Rev. B* **92**, 174113 (2015).
 - [S2] D. G. Matei, T. Legero, C. Grebing, S. Häfner, C. Lisdat, R. Weyrich, W. Zhang, L. Sonderhouse, J. M. Robinson, F. Riehle, J. Ye, and U. Sterr, *J. Phys.: Conf. Ser.* **723**, 012031 (2016).
 - [S3] G. Rupschus, R. Niepraschk, K. Jousten, and M. Kühne, *J. Vacc. Sci. Tech. A* **12**, 1686 (1994).
 - [S4] C. Hagemann, C. Grebing, T. Kessler, S. Falke, N. Lemke, C. Lisdat, H. Schnatz, F. Riehle, and U. Sterr, *IEEE Trans. Instrum. Meas.* **62**, 1556 (2013).
 - [S5] D. W. Allan and J. Barnes, in *Proceedings of the 35th Ann. Freq. Control Symposium* (Electronic Industries Association, Ft. Monmouth, NJ 07703, 1981) pp. 470–475, for corrections see [S20].
 - [S6] E. Benkler, C. Lisdat, and U. Sterr, *Metrologia* **52**, 565 (2015).
 - [S7] E. Rubiola, *Rev. Sci. Instrum.* **76**, 054703 (2005).
 - [S8] S. T. Dawkins, J. J. McFerran, and A. N. Luiten, *IEEE Trans. Ultrason. Ferroelectr. Freq. Control* **54**, 918 (2007).
 - [S9] G. Kramer and W. Klische, in *Proceedings of the 18th European Frequency and Time Forum, Guildford, UK* (IET, London, UK, 2004) pp. 595–602.
 - [S10] D. W. Allan, *IEEE Trans. Instrum. Meas.* **IM-36**, 646 (1987).
 - [S11] G. M. Stephan, T. T. Tam, S. Blin, P. Besnard, and M. Tetu, *Phys. Rev. A* **71**, 043809 (2005).
 - [S12] M. Bishof, X. Zhang, M. J. Martin, and J. Ye, *Phys. Rev. Lett.* **111**, 093604 (2013).
 - [S13] F. J. Harris, *Proc. IEEE* **66**, 51 (1978).
 - [S14] N. Von Bandel, M. Myara, M. Sellahi, T. Souici, R. Dardailon, and P. Signoret, *Opt. Express* **24**, 27961 (2016).
 - [S15] D. A. Steck, *Quantum and Atom Optics* (available online at <http://steck.us/teaching> (revision 0.11.5, 27 November 2016), 2016).
 - [S16] B. E. A. Saleh and M. C. Teich, *Fundamentals of Pho-*

- tonics* (John Wiley & Sons, Inc., New York, New York, 1991).
- [S17] W. Klemperer, Proc. IEEE **60**, 602 (1972).
- [S18] A. E. E. Rogers and J. M. Moran, Jr., IEEE Trans. Instrum. Meas. **30**, 283 (1981).
- [S19] A. R. Thompson, J. M. Moran, and G. W. Swenson, *Interferometry and Synthesis in Radio Astronomy* (Wiley, New York, 2007).
- [S20] D. Sullivan, D. Allan, D. Howe, and F. Walls, *Characterization of Clocks and Oscillators*, NIST Tech. Note 1337 (NIST, U.S Department of Commerce, National Institute of Standards and Technology, 1990) online available at <http://tf.nist.gov/cgi-bin/showpubs.pl>.